Phase Transition and Related Phenomena in Chemically Deposited Polycrystalline Cadmium Sulfide Thin Films

Daniel Lincot* and Bandombele Mokili

Laboratoire d'Electrochimie et de Chimie Analytique (Unité associée au CNRS), Ecole Nationale Supérieure de Chimie de Paris, 11 rue Pierre et Marie Curie, 75231 Paris Cedex 05, France

Michel Froment, Robert Cortès, and Marie Claude Bernard

Laboratoire de Physique des Liquides et Electrochimie (UPR 15 du CNRS), Université Pierre et Marie Curie, 4 place Jussieu, 75252 Paris Cedex 05, France

Catherine Witz and Jacques Lafait

Laboratoire d'Optique des Solides (CNRS), Université Pierre et Marie Curie, 4 place Jussieu, 75252 Paris Cedex 05, France

Received: August 8, 1996; In Final Form: October 29, 1996[⊗]

Optical and structural properties of chemically deposited CdS films have been characterized by using spectroscopic ellipsometry and electron transmission microscopy. Three representative cases have been studied using grown metastable cubic film and two films annealed at 400 °C (30 min) with and without a $CdCl_2$ pretreatment (2 min dip in a $CdCl_2$-saturated methanol solution). Without the pretreatment, the film remains at an intermediate state between the cubic and the stable hexagonal structure. With the pretreatment, a full transition to the hexagonal structure along with a strong recrystallization takes place. Full cubic or hexagonal films present high band gap values (2.44−2.46 eV), whereas band gap narrowing by ≈0.1 eV is observed in the second case. This effect is shown to be associated to a spatially modulated structure with a high density of stacking faults. This structure can be identified as a polytype cubic/hexagonal structure, which is a metastable intermediate in the phase transition process. Possible origins of the associated band gap lowering as order/disorder transition or stress effects are discussed.

Introduction

Cadmium sulfide is an important semiconductor for basic physical studies and applications in optoelectronic devices. Thin films have been prepared from the gas phase by physical deposition methods such as coevaporation, sputtering, molecular beam epitaxy, and by chemical methods including chemical vapor deposition and spray pyrolysis. It is also possible to deposit films chemically from aqueous solutions,[1−3] and this method is named chemical bath deposition (CBD) by analogy with chemical vapor deposition (CVD). Recently this deposition technique found a renewed interest in the field of photovoltaics.[4] It emerges also for the passivation of optoelectronic devices.[5]

The preparation in a liquid environment, at near room temperature, and the use of dissolved precursors in a ionic medium may help us better choose desired specific properties than preparation from the gas phase. The relations between the internal structure and the preparation and/or the annealing conditions and the properties of the films are an open field of investigation. Recently, the phase transition from cubic to hexagonal films was evidenced after annealing treatments of grown films.[6] The transition characteristics were shown to depend strongly on the annealing conditions and atmosphere: it starts to take place at about 300 °C in an argon−sulfur atmosphere after 28 h but does not in argon or air under the same conditions.[6c] A parallel finding is that band gap variations are observed with the presence of a sharp minimum (from 2.43 to 2.25 eV) in an intermediate temperature range (300 °C).[6b] This minimum has been attributed to an increase of the lattice constant[6d] and, subsequently, to a defect formation during the phase transition.[6e] The cubic to hexagonal transition was also observed in CdS quantum dots under annealing in argon at $T > 300$ °C with a parallel increase of the grain size.[7] A phase transition from cubic to hexagonal modification has been also reported for CdS films deposited by molecular beam epitaxy on (110) InP beyond a critical thickness of 200 nm.[8] These phenomena are a consequence of the polymorphism of CdS, which exhibits either the cubic or the hexagonal modification, with close formation energies. The hexagonal structure is slightly more stable with $\Delta E_{W-ZB} = -1.1$ meV/atom.[9]

The polymorphism of CdS is also observed for grown CBD films. As a function of the deposition conditions or substrates, the cubic or hexagonal modifications[10,11] are observed. This also true for CBD epitaxial films on InP as a function of the substrate orientation (hexagonal on $(\bar{1}\bar{1}\bar{1})$ InP,[11a] cubic on (100) InP[11b]).

In this paper we further analyze the phase transition processes in CBD CdS films with a main focus on microstructural characterizations by electron transmission microscopy techniques in relation to optical properties.

In a previous work, we found that the deposition of CdS on silicon resulted in the formation of polycrystalline films with the cubic structure.[11a] As silicon is an excellent substrate for further characterizations, this gives us the opportunity to use these films to study the transition to the hexagonal phase and the related phenomena occurring during well-selected thermal annealing treatments. We have selected two different annealing treatments allowing us to obtain a mixed cubic/hexagonal structure and a pure hexagonal structure, respectively. Adding

[⊗] Abstract published in *Advance ACS Abstracts,* February 1, 1997.

S1089-5647(96)02399-1 CCC: $14.00

the deposited film, which is cubic, gives us the three most representative cases. The mixed hexagonal/cubic structure is obtained by an annealing treatment in argon, and the hexagonal structure is obtained in the same conditions but in the presence of a strong recrystallization agent, $CdCl_2$, which is widely used in CdS/CdTe cells processing.[12a] NaCl has been also observed to enhance the phase transition of cubic CdS powders.[12b]

The properties are then investigated and compared by using spectroscopic ellipsometry, X-ray diffraction (XRD), Rutherford backscattering spectroscoscopy (RBS), Raman spectroscopy, transmission electron microscopy (TEM), and high resolution TEM (HREM) for structural characterizations at the atomic level. By using this approach the modifications of the optical properties determined by ellipsometry are directly related to the structural changes. This demonstrates that the transition between cubic and hexagonal structures takes place with the formation of polytype CdS and that the band gap lowering is associated with this metastable polytype structure, probably in relation to induced disorder or stress effects.

Experimental Section

Deposition Conditions. Undoped silicon wafers, (111) oriented, are used as substrates. After degreasing with acetone, the surface SiO_2 layer is removed by dipping the wafers in a HF/KF solution with a pH of 4.5, at room temperature, for 3 min. After the substrates are rinsed with deionized water, they are introduced into the reaction vessel. The composition of the deposition bath for CdS consists of 1.74M of NH_3 introduced as ammonium hydroxide with 0.015 M of NH_4^+ ions introduced as $(NH_4)_2SO_4$ salt, 0.01M of $CdSO_4$, and 0.1 M of thiourea ($SC(NH_2)_2$). A deposition time of 15 min at 60 °C resulted in a film about 0.1 μm thick.

Two different thermal annealing treatments were performed. The first one was made in an argon atmosphere at 400 °C for 0.5 h (annealing 1, denoted R1). The second one was made in air in the same conditions (400 °C for 0.5 h), but the CdS film was previously dipped for 2 min in a methanol solution at room temperature containing dissolved cadmium chloride under saturation conditions (annealing 2, denoted R2). This leads to the deposition of a very thin layer of cadmium chloride on the CdS surface. The fact that the annealing treatment is then made in air or in argon has no influence on the final results.

Characterization Techniques. The optical properties have been essentially determined by spectroscopic ellipsometry using a rotating polariser ellipsometer ES4G from SOPRA, working in the spectral range from 270 to 900 nm. This technique allows one to extract the ellipsometric parameters tan Ψ and cos Δ from the Fourier transform of the intensity coming from the analyser (Hadamard method). The complex index of refraction of the CdS layer $\tilde{n}(\lambda) = n + ik$ is then calculated by considering that the interface structure is the following: inhomogeneous effective layer of CdS (representing the surface rugosity) + homogeneous CdS layer (n, k, and thickness d) + SiO_2 thin layer (2nm) + Si substrate (semiinfinite).

Raman spectra were recorded using a DILOR multichannel Raman spectrometer with the 514.5 nm line of an argon ion laser focused onto the sample through a microscope, in a backscattering geometry. The laser source was operated at a nominal output of 20mW. The spectral resolution was about 3 cm^{-1}.

Transmission electron microscopy (TEM) was performed using a Jeol 100 CXII apparatus for routine examinations. High-resolution imaging (HREM) was achieved using a 200 kV Philips CM 20 microscope. The silicon substrates were first mechanically thinned, then ion milling allowed us to eliminate silicon, stopping when CdS was reached.

TABLE 1: Analysis of the Film Composition and Thickness Evaluation by RBS. Annealing 1 and 2: See Text

	grown	annealing 1	annealing 2
Cd concn no. of atoms/cm^2	153×10^{15}	160×10^{15}	157×10^{15}
O concn	44×10^{15}	27×10^{15}	28×10^{15}
Cd/S ratio	1.1	1.09	1.12
RBS thickness/nm	77	80	78

X-ray diffraction (XRD) allows us to quantitative evaluate the structure of the films. Measurements were taken using an XRD goniometer specially designed for thin film studies and a Cu Kα source. A LiF flat monochromator crystal and a NaI-(Tl) detector associated with a discriminator pulse height analyzer were used. The entrance slit (1×0.05 mm^2) vertically defines a very narrow beam and allows us to impinge a 10 mm of diameter sample under a glancing angle. With a glancing angle of 0.6°, the X-ray path in the film is multiplied by a factor 100, therefore, the film X-ray absorption is about 20% for a 20 nm film thickness. The sample is fixed, and the detector is displaced for the determination of the diffraction angle 2θ. The goniometer position is controlled by a microcomputer, which measures the position and the intensities of the selected Bragg peaks.

Nuclear microanalysis was used to determine the composition of the films before and after the annealing treatments. The amounts of cadmium and sulfur were determined by $^4He^+$ Rutherford backscattering spectrometry (RBS). In some cases, the oxygen content was measured using the $^{16}O(d,p)^{17}O^*$ nuclear reaction. In both cases, absolute values were obtained by comparison with a reference target. The error is about 2%.

Results

Composition of the Films. In Table 1 are shown composition determinations made on the films by RBS before and after annealing 1 and annealing 2. Within the error margin there is no change of the cadmium and sulfur absolute concentrations before and after the annealing treatments. The ratio Cd/S is about 1.1 instead of unity for stoichiometric films. Such deviations of stoichiometry are well-known in chemically deposited CdS films. They are attributed to the presence of additional cadmium compounds as $Cd(OH)_2$,[13a,b] or $CdCN_2$.[13a] The presence of the carbonate group has been also reported.[13c] In our case, oxygen is present in the films, but no significant amounts of carbon or nitrogen are found. The ground level of oxygen on Si substrates after HF/KF etching is 2.3×10^{15} cm^{-2}, indicating that the measured values are really related to oxygen in the film. The amount of oxygen ($\approx 30.0 \times 10^{15}$ cm^{-2}) determined after annealing is about two times the excess of cadmium atoms ($\approx 15.0 \times 10^{15}$ cm^{-2}), which is consistent with the presence of cadmium hydroxide as the supplementary species in the film. In the grown films, the oxygen content is slightly higher. This is due to the presence of adsorbed water, which is easily removed by heating as shown by parallel infrared measurements (not shown). The presence of cadmium hydroxide species can be explained by the deposition mechanism which involves adsorbed cadmium hydroxide intermediate reaction species.[3] It varies with deposition conditions.[13a,b] The thickness of the films, evaluated from the surface concentration of cadmium atoms while assuming pure CdS, are indicated in Table 1. No significant change is observed after the different treatments.

Ellipsometric Measurements. The complex optical index has been derived from ellipsometric measurements by using a procedure which considers that the film is made of two layers, an inner compact layer and an outer layer accounting for the

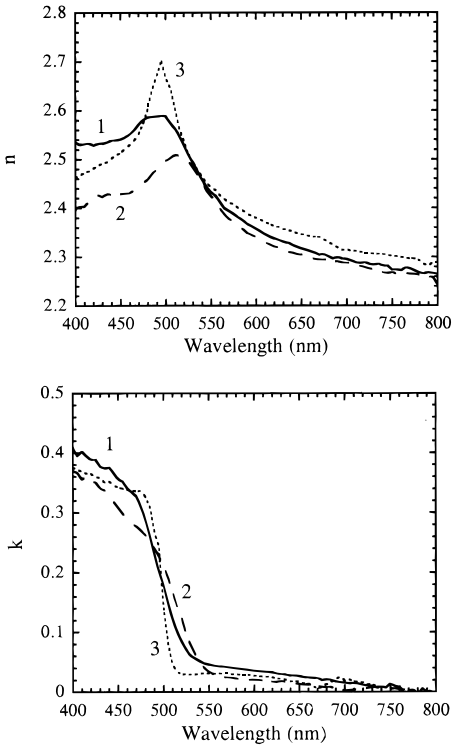

Figure 1. Refractive index (top) and absorption index *k* (bottom) as a function of wavelength determined by ellipsometry for CdS layers deposited on silicon: (1) grown film deposited in an ammonia solution, (2) after annealing 1 (400 °C, 30 min, argon), (3) after annealing 2 (400 °C, 30 min, air) in presence of $CdCl_2$ (see text).

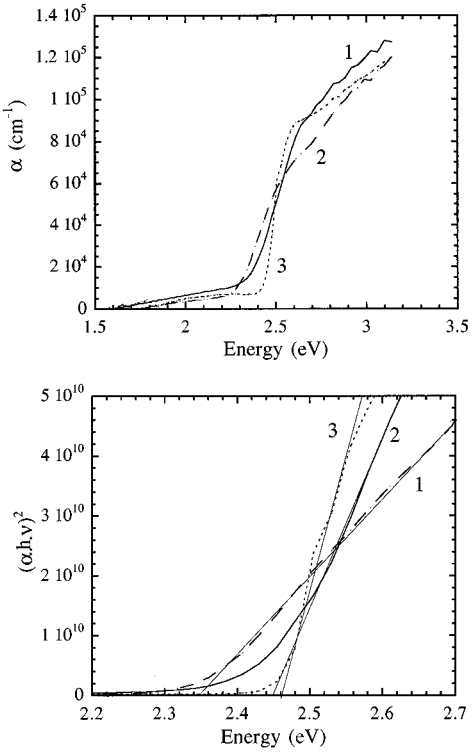

Figure 2. (a) Absorption coefficient (α) as a function of the energy obtained from results of Figure 1b. Lines 1, 2, and 3 correspond to the layers presented in Figure 1. (b) $(\alpha h\nu)^2$ as a function of the energy. The lines correspond to linear fits, allowing band gap determination.

TABLE 2: Influence of Annealing Conditions on the Parameter Values Obtained from Ellipsometry (See Text). d_0: Thickness Determined with a Mechanical Profilometer

sample	d_0 (nm)	d (nm)	d_r (nm)	p_r (nm)	d_1 (nm)
grown	88.0	76.7	16.6	0.84	93.3
annealing 1	88.0	85.6	7.4	0.24	93.0
annealing 2	75.0	70.8	17.9	0.63	88.7

surface rugosity. For the later part, an effective medium is considered with a mixture of air and of the compact layer material.

Table 2 summarizes the results of this calculation. d_0 is the thickness of the film determined using a mechanical profilometer and d and d_r are the thicknesses of the compact layer and the rough layer determined from the treatment of the ellipsometric data. The CdS volume fraction in the rough layer is indicated as p_r. $d_1 = d + d_r$ is the total thickness from the ellipsometric measurements.

The thicknesses determined by the optical procedure are in good agreement with those determined mechanically with $d < d_0 < d_1$. The agreement is also good with the estimations which can be made from the RBS determinations (Table 1). Whereas the total thickness is not changed significantly, variations appear for the dense and rough layers thicknesses. The annealing without cadmium chloride appears to increase the density of the film, which is the opposite for the annealing in the presence of cadmium chloride.

Figure 1 shows the calculated optical indexes (*n* and *k*) as a function of wavelength for the three samples (CdS0, CdSR1, and CdSR2). The curves are similar to those measured on evaporated films.[14] *n* values (Figure 1a) tend to increase for the film treated with cadmium chloride. Differences also appear in the peak position and width. The peak is shifted towards higher wavelengths (lower energies) for the sample annealed without cadmium chloride. An important reduction of the width takes place for the film annealed with cadmium chloride. Changes appear on the absorption index curves (Figure 1b) especially in the 450−550 nm region corresponding to the absorption onset range. The absorption onset is shifted toward higher wavelength values after annealing 1 (CdSR1) and to lower after annealing 2 (CdSR2), together with an increased steepness in this case. This behavior is concomitent with the variation of the peak position and the shape of the refractive index curve.

From the *k* values the absorption coefficient α is calculated using the relation $\alpha = 4\pi k/\lambda$. Figure 2a shows the absorption coefficient (α) as a function of the photon energy for the different samples. The plots $(\alpha h\nu)^2 = f(h\nu)$ are shown in Figure 2b. The band gap values, as determined by the extrapolation of the linear parts, are 2.45 eV for the grown film, 2.34 eV for the film after annealing 1, and 2.46 eV for the film after annealing 2. As a consequence, a band gap narrowing effect is clearly evidenced after annealing 1. Changes in the slope are also evidenced and reflect the differences of steepness of the absorption onset already mentioned from the $k = f(\lambda)$ curves. The ellipsometric study confirms results obtained from photocurrent and electrotransmittance analysis using the semiconductor/electrolyte junction.[15]

Raman Spectroscopy. Figure 3 shows the Raman spectra of the chemically deposited CdS films after base line correction in case b, for the sample annealed without $CdCl_2$. The peaks at 305 and 601 cm^{-1} correspond to the vibrations of longitudinal optical phonons (LO) and (2LO) of CdS.[16a] The 520 cm^{-1} peak is due to the Si substrate. For the two annealed samples, the LO peak is slightly sharper (FWHM = 20 cm^{-1} for the deposited film and FWHM = 17 and 15 cm^{-1} after annealings 1 and 2). Annealing 1 leads to the highest intensity LO peak and the highest ratio relative to the peak of Si. A strong increase of the background toward higher wavenumbers is also observed. The increase of the Raman signal and of the background are

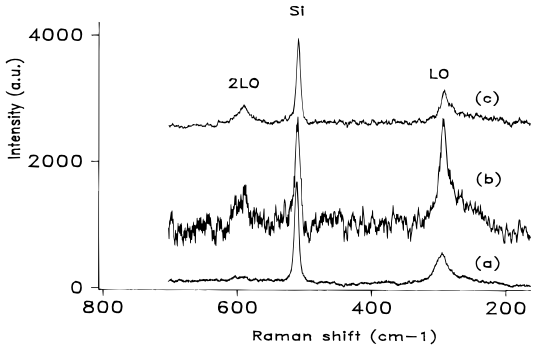

Figure 3. Raman spectra of CdS films deposited on silicon: (a) as grown film deposited in an ammonia solution (see text), (b) after annealing 1 (400 °C in argon for 0.5 h), (c) after annealing 2 (400 °C in air for 0.5 h) in presence of $CdCl_2$ (see text).

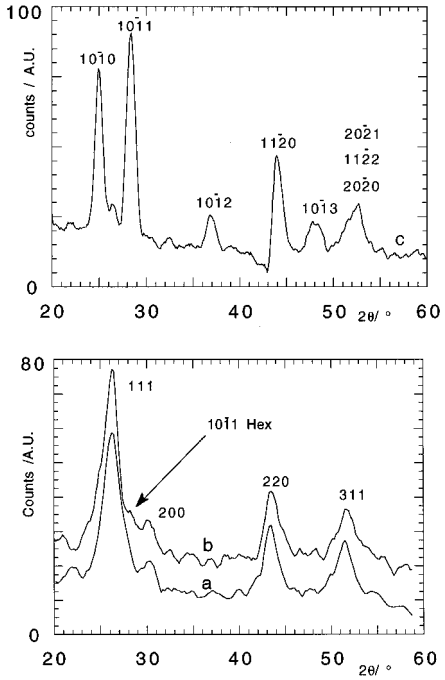

Figure 4. Glazing incidence XRD spectra of CdS films on Si (111): (a) As grown film, (b) after annealing 1, (c) after annealing 2 in presence of $CdCl_2$. The peaks are indexed with the cubic modification of CdS in (a) and (b) and with the hexagonal modification of CdS in (c).

characteristic of resonance effects appearing when the excitation energy is closer to the band gap.[16b] In this case, the incident photon energy is 2.41 eV, which is lower than the band gap values of grown and annealed 2 samples (2.45 and 2.46 eV) but is higher than the value for the annealed 1 sample (2.34 eV). The presence of enhanced cross sections near resonance for CdS has been already reported.[16b] For the 2LO peaks, a higher intensity is observed for the two annealed samples, especially for $CdCl_2$ annealed one. The changes in the 2LO/LO ratio are likely to reflect changes in the CdS electronic structure.[16c]

Structural Studies

XRD. In Figure 4 are shown the indexed XRD spectra of the film under the three different conditions. Grown (sample CdS0) and annealed 1 (sample CdSR1) films are cleary identified as mainly cubic. After annealing 1, a slight modification of the spectrum takes places with the appearance of additional peaks of smaller intensity. The small hump appearing at about 28° may be ascribed to the (10$\bar{1}$1) peak of the hexagonal structure. From the relative amplitudes the proportion of hexagonal CdS should be at the level of a few per cent. After annealing 2 (sample CdSR2), complete vanishing of the cubic spectrum takes place and a new pattern appears which corresponds to hexagonal CdS. Thus, a complete reorganization of the film has taken place after annealing 2.

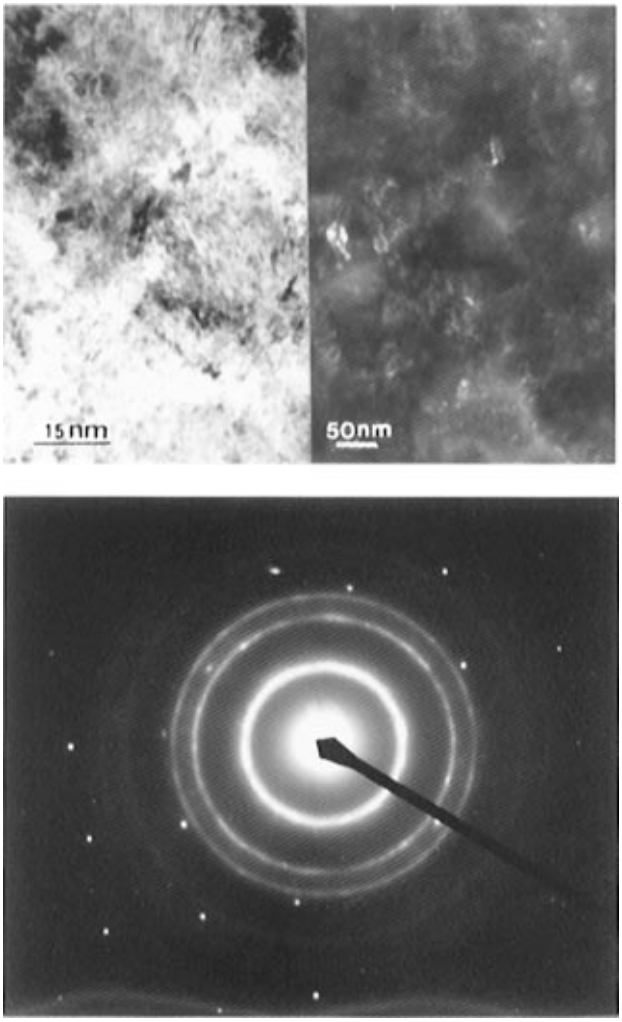

Figure 5. Structure of a grown CdS film: (top left) TEM image, (top right) Dark Field TEM image, (bottom) SAD pattern corresponding to the cubic blende modification.

Electron Transmission Studies. XRD studies show that a cubic to hexagonal phase transition occurs with annealing 2 but that that structural changes are hardly seen between grown and annealed 1 films despite major differences in the optical properties. More precise analysis of the structural changes has been carried out by means of TEM images and selective area diffraction (SAD) patterns. Figures 5, 6, and 7 show the results obtained for the three samples. Figure 5a shows the TEM image of the grown CdS (sample a). It presents a fleecy aspect which is homogeneous. From the ellipsometric results, we know that the layer is also compact. The interesting point is that individual grains or grain boundaries are hardly seen, in particular no spherical nodules appear as are generally seen for films made by the aggregation of colloids. Black and white stripes, corresponding to extended defects, can be observed in some places with an apparent density of 5.0×10^{11} cm cm^{-2} (total length of defect (cm) per unit area (cm^{-2})). Dark field images (Figure 5b) allow us to determine grain sizes in the range of 30−50 nm. The film is made of strongly overlapping grains.

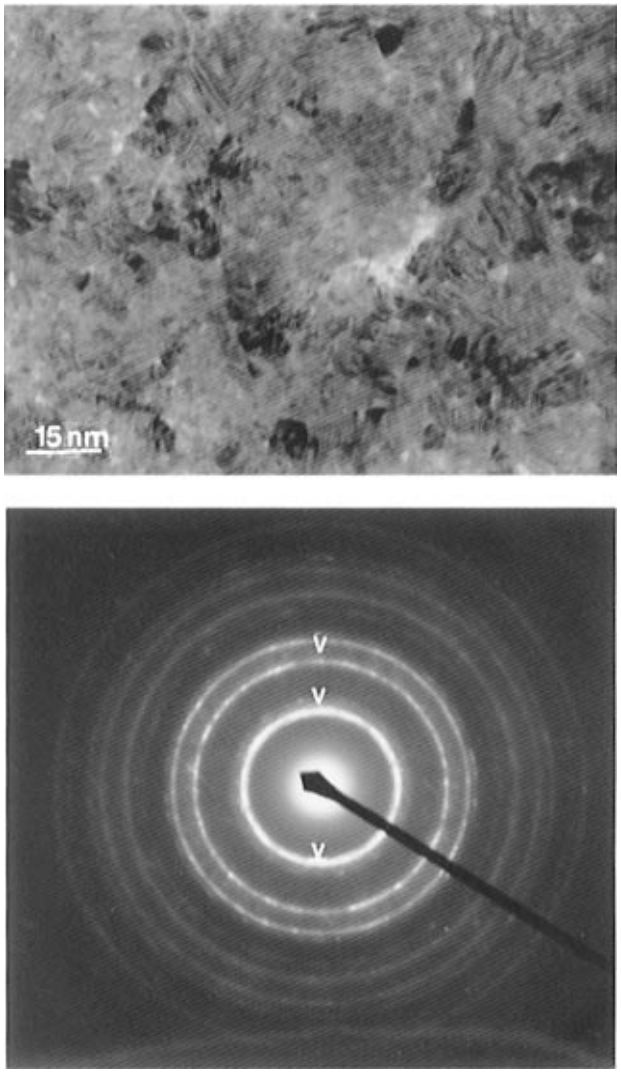

Figure 6. Structure of a CdS film after annealing 1: (a) TEM image showing a high density of twins and stacking faults, (b) SAD pattern corresponding to the cubic Blende structure with some additional rings indicated by arrows and corresponding to the hexagonal modification.

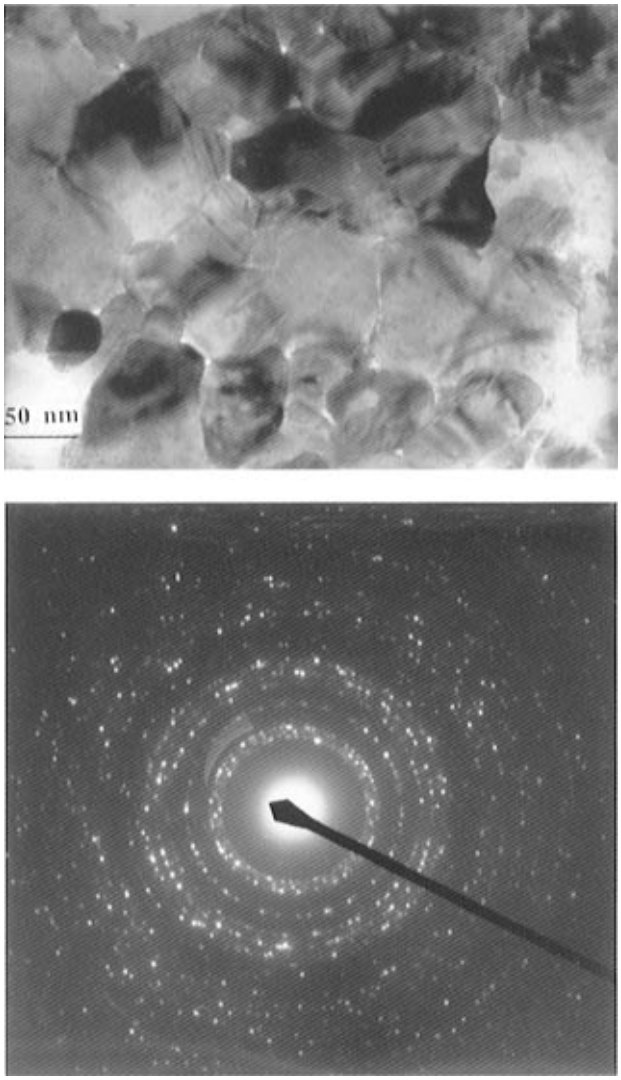

Figure 7. Stucture of a CdS film after annealing 2: (a) TEM image showing a strong recrystallization of the film, (b) SAD pattern corresponding to the hexagonal modification. The dot pattern indicates the increaze of the grain size as compared to the two previous cases.

The SAD pattern (Figure 5c) corresponds to the cubic structure, in agreement with the XRD analysis. After annealing 1, a change of the structural state is observed (Figure 6a). The film has lost its hazy aspect and the grain structure appears more clearly. However, from dark field imaging (not shown), only a slight increase of the grain size is observed (50−70 nm). The most striking change is the dramatic increase of the density of extended planar defects like twins or stacking faults, with a value of about 10^{13} cm cm^{-2}. The SAD pattern (Figure 6b) still shows a ring pattern corresponding to the a cubic structure, but weaker intensity rings appear, indicated by the arrows. Their position correspond to the hexagonal modification of CdS. This indicates that a phase transition has started in the layer.

In contrast to annealing 1, annealing 2 produces a spectacular recrystallization with a grain size approaching 90 nm. Some grains have regular hexagonal shapes (Figure 7a). The density of planar extended defects is very low (10^{11} cm cm^{-2}). Some SAD pattern (Figure 7b) is now characteristic of the hexagonal structure; no reflexion belonging to the cubic structure is observed. The increase of the grain size explains the observation of a dot pattern instead of a ring pattern for the other cases.

HRTEM brings supplementary information on the structural organization of the CdS films. Despite its hazy apparence from TEM observations, HRTEM images of the grown samples show its local crystalline structure and areas where projections of atomic columns can be observed (Figure 8). Figure 8a shows a typical HRTEM image and the Fourier transform diffraction pattern (inset). This pattern corresponds to the major cubic modification. The presence of streaks is related to planar extended defects, the density of which being estimated at 5×10^{11}cm cm^{-2}. The distance between atomic rows along [011] direction is indicated on the image. In contrast to the SAD patterns, which are attributed only to the cubic structure, some minor areas present an hexagonal arrangement. Figure 8b presents such an area and the corresponding Fourier transform diagram (inset). The Fourier transform diagram corresponds now to the hexagonal structure, and the image is the atomic column projection on the (0001) basal plane. After annealing 1, the main difference with the grown film is a strong increase in the stacking fault density, appearing as black and white stripes inside individual grains (Figure 6a). Figure 9a shows at a extended scale the structure of these defects, which appear as a rather regular parallel juxtaposition of thin domains of a few nanometers width with rotated atomic directions from one to the other. In other places, intersecting extended defects can be observed instead of the previous structure. An example is shown in Figure 9b. These defects are formed during the thermal treatment. The appearance of the hexagonal reflections in the diffraction pattern indicates that hexagonal domains are formed in relation to the stacking faults. After annealing 2,

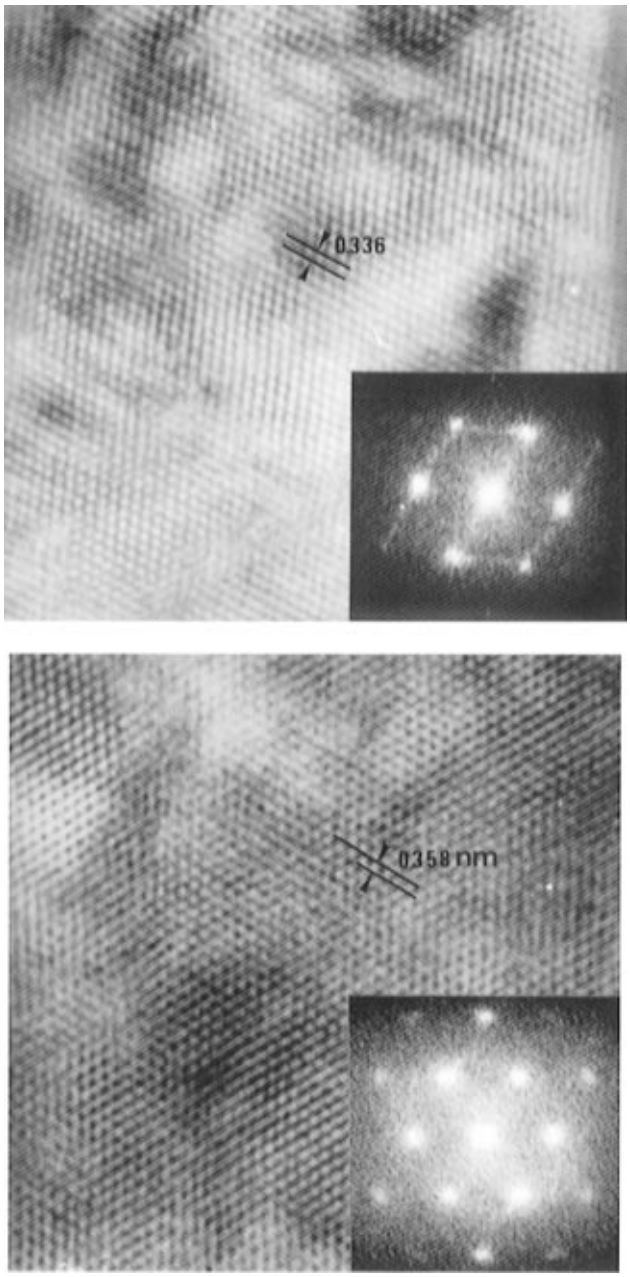

Figure 8. HREM observations of a grown CdS film. (a) HREM image, (inset): Fourier transform diffraction pattern corresponding to the majoritary cubic blende structure. Note the presence of streaks indicating the presence of defects. (b) HREM image, (inset): Fourier transform diffraction pattern corresponding to the hexagonal structure. This is observed in some places of the layer.

large areas inside the grains give HREM images with no stacking fault. Figure 10a reveals $(10\bar{1}0)$ planes (0.358 nm) and an atomic projection on the (0001) plane. In some grains a periodicity of 0.671 nm has been also found (Figure 10b) and corresponds to the c parameter of the CdS hexagonal structure. These images can be interpreted as a projection of atomic columns along the $[11\bar{2}0]$ direction.

Discussion

It has been recently shown[6] that the transition between cubic to hexagonal modifications in chemically deposited films as a function of the annealing temperature resulted in a non-monotonic variation of the band gap values, with the presence of a sharp minimum in the $Eg = f(T)$ curve situated at about 250 °C. In other papers, a decrease of the band gap has been

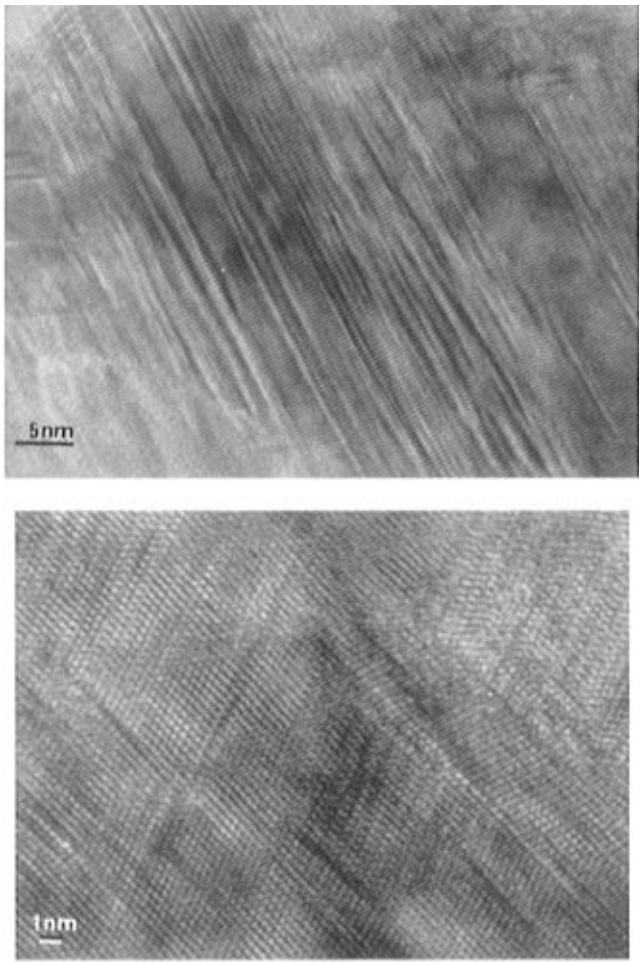

Figure 9. HREM image of a CdS film after annealing 1: (a) internal structure of a grain presenting parallel stripes corresponding to stacking faults with alternance of cubic and hexagonal structures (polytypic structure). These grains appear with a great density in the low magification image in Figure 6. (b) Other type of perturbated intra grain structure with stacking faults networks.

also reported for annealing treatments up to 400 °C in air.[15] This indicates that a common phenomenon is probably responsible for this effect. Our results allow us to reject an interpretation based on compositional changes (with the formation of cadmium oxide for instance); and we think the effect is more likely a consequence of the transition processes between cubic and hexagonal structures.

We show that the intermediate state of the phase transition process is characterized by the presence of a high density of extended defects which are not present in the two extreme cases (full cubic or full hexagonal). These defects correspond to stripes of a few nanometers in width and a few tens of a nanometer long appearing in a quasi periodic form in individual grains, as shown in Figure 6a and at the atomic scale on Figure 9a. These defects, parallel to the (111) plane of the cubic structrure or the basal (0001) planes of the hexagonal structure, find their origin in the formation of stacking faults. It is known for a long time[17] that the presence of a stacking fault in a cubic structure (respectively hexagonal) creates a lamella presenting the hexagonal (respectively cubic) arrangment as shown in Figure 11 in the case of a hexagonal structure. The arrow indicates the position of the stacking fault. As a consequence, the extended defects correspond to successive regions of cubic and hexagonal structures. This explains the appearance of hexagonal reflections in the electron diffraction and XRD patterns.

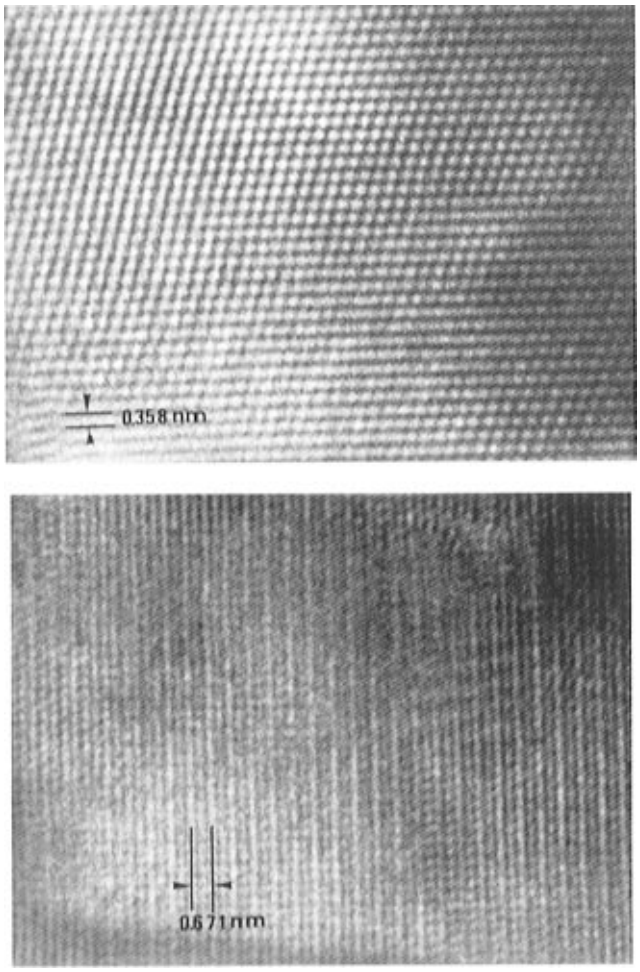

Figure 10. HREM observation of a CdS film after annealing 2; (a) the image is a projection of atomic columns on the (0001) plane of the hexagonal structure. The distance between the arrows corresponds to the spacing between $(10\bar{1}0)$ planes. (b) The image is a projection along the $[11\bar{2}0]$ direction. The distance between the arrows corresponds to the *c* parameter of the hexagonal structure.

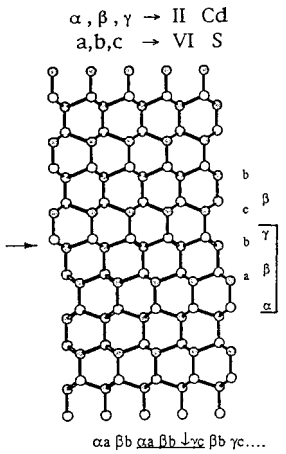

Figure 11. Mechanism of formation of polytype structures in CdS; lamellae of cubic structure are represented in an hexagonal structure between two stacking faults parallel to the (111) cubic planes or (0001) hexagonal planes.[23]

Such structures are also known as polytype structures. They have been extensively studied for various compound materials, in particular SiC,[18,19] and ZnS.[20] In the cases of CdS[21] and CdSe,[22] the occurrence of polytypism has been demonstrated, but the amount of literature is much larger for ZnS. In ZnS, the phase transformation takes place from the hexagonal to the cubic phase (slighly more stable, by −3.1 meV/atom[9]). It has been demonstrated that this phenomenon involves the formation of polytype structures.[20] Polytypes can be defined by the stacking sequence of (111) or (0001) atomic planes with respect to the three possible positions ABC. The cubic structure is noted 3C, and corresponds to the sequence ABCABCABC... The hexagonal structure is noted 2H, and corresponds to the sequence ABABABABAB... A polytype is noted *n*H or *n*C, where *n* represents the number of planes in the unit cell and H or C the host structure. An example of a short period polytype structure is ABCACBABCACBABC noted 6H. This polytype is simply obtained by a permutation of a sequence BC in the cubic arrangment[18] as indicated by underlining. By further permutations it is possible to reach the hexagonal arrangment.[20c] Despite the fact that tens of polytype structures are possible in ZnS,[20a,b] only certain arrangments are observed corresponding to the more metastable configurations, which have been simulated by numerical models.[20a,b] During the phase transformation process, the hexagonality factor *h* varies from 0 to 1 (or 1 to 0) via a sequence of consecutive polytypes (for 4H, $h = 0.5$). Our results show that these mechanisms also take place for CdS. From the results some grains have reached the polytype structure (Figure 9a), while some others seem to be at an anterior state (Figure 9b). The polytype in Figure 9a is more likely a short period polytype (1−3 nm cell unit). This is in agreement with the results of Prasad et al.[21a] who found that 4H (*c* = 3D 1.344 nm) and 6H (*c* = 3D 2.016 nm) occur most frequently.

The effect of atmosphere is well demonstrated in this work by the comparison between the annealing with and without $CdCl_2$. The former annealing only leads to a polytype intermediate, whereas the latter annealing leads to the complete transformation. This emphasizes the role of $CdCl_2$ as promotor of crystallization allowing grain growth. In this work, we show in addition that it accelerates the transformation cubic to hexagonal in individual grains. This may result from a change in the surface properties of the grains (surface tension and composition) while changing the velocity of individual phase domain transformations. As compared with published results[6] this kind of chemical activation is more efficient to promote phase transformation in CdS than using only the temperature parameter or sulfur atmosphere. This agrees with a previous study of the kinetics of recrystallization of CdS powders in presence of NaCl.[12b]

Considering now the band gap variations, it is known that the values for cubic and hexagonal CdS are essentially the same within 0.1 eV.[8,23] Our results are in agreement with this finding with $E_g \approx 2.45$ eV for the cubic film (grown) and 2.46 eV for the hexagonal film (annealing 2). As a consequence, the lower band gap values should be due to the properties of the polytypes, since variations of composition are not important (Table 1). In the case of SiC, different band gaps are observed for the different polytypes.[19] If CdS follows the behavior of SiC, one should expect only small band gap variations between the two extreme values since they are close together and the presence of a sharp minimum can be hardly explained. In the case of the phase transition of ZnS, an intermediate disordered structure state is found,[24] with an hexagonality factor of 0.5. For CdS a disordered intermediate is also mentioned.[21b] According to this mechanism, one could expect a band gap narrowing effect associated to a disordered structure and the existence of a sharp minimum of the band gap as a function of the hexagonality factor. This minimum corresponds to the maximum density of stacking faults and related to maximum disorder and/or defect creation (pairs of structural defects have been discussed in[6e]). On both sizes of the minimun gap value the reduction of the

Figure 12. HREM image of a grown CdS film prepared from different deposition conditions ([CdSO4] = 0.01 M − [thiourea] = 0.028 M, ammonia 1.7 M, and T = 60 °C) presenting an intragrain structure similar to that observed after annealing 1 (Figure 9b).

stacking fault density leads to a progressive reduction of the local disorder and to an increase of the gap to the pure phase values. Figure 9 shows that in addition there are some deformations and disorientations in the stripes, which are not completely parallel. This can also induce strains in the layer, which are also factors which have a direct effect on the gap value. De Melo et al.[6] report a slight increase of the lattice parameter at the minimum gap value. From our measurements it was not possible to detect a change in the lattice parameter of the intermediate low band gap state.

The effect we describe here for CdS can be compared with band gap variations with the presence of a minimum reported for $GaInP_2$ layers deposited at different temperatures.[25] Similar to CdS, these variations are associated to a structural transition involving also an intermediate state characterized by the alternance of different crystallographic domains.

At this stage it is interesting to recall that CdS polymorphism is also observed in grown CBD films. Stacking faults and polytypic structures similar to those described here have been observed with densities depending on the deposition conditions.[26a] In some cases, pure hexagonal phase films can be prepared.[26b] The presence of stacking faults can be also detected in some grains in the grown film of this study (Figure 5a). Figure 12 shows that structures similar to those shown in Figure 9b, which do not consist in well-separated lamellae, can be observed in grown films. This points out the similarity between the effect ot temperature and that of the deposition conditions and suggests that all intermediate states can be obtained directly in solution. This may be an explanation for the band gap variations observed in grown films.[10b,15a]

Conclusion

In this work, optical and structural properties of chemically deposited CdS films have been characterized by using ellipsometry, XRD, and HRTEM. Three representative samples have been selected, allowing us to address the question of polymorphism and polytype formation in CdS layers. We propose a direct relation between these effects and the observed variations of the optical properties of the film. Possible origins of these variations are order/disorder transitions inducing the creation of defects or stress. These effects also appear in grown films.

Acknowledgment. D. Lincot and B. Mokili acknowledge the support of the European Union in the frame of the JOULE-EUROCAD Project (Grant JO42-CT92-0243).

References and Notes

(1) Kitaev, G. A.; Uritskaya, A. A.; Mokrushin, S. G. *Russ. J. Phys. Chem. Transl. Zh. Fiz. Thin.* **1965**, *39*, 1101.

(2) Chopra, K. L.; Kainthla, R. C.; Pandya, D. K.; Thakoor, A. P. *Phys. Thin Films* **1982**, *12*, 167 and references therein.

(3) Ortega-Borges, R.; Lincot, D. *J. Electrochem. Soc.* **1993**, *140*, 3464.

(4) (a) Stolt, L.; Hedström, J.; Kessler, J.; Ruckh, M.; Velthaus, K. O.; Schock, H. *Appl. Phys. Lett.* **1993**, *62*, 597. (b) Britt, J.; Ferekides, C. *Appl. Phys. Lett.* **1993,** *62*, 2851.

(5) Vaccaro, K.; Davis, A.; Dauplaise, H. M., Spaziani, S. M.; Martin, E. A., Lorenzo, J. P. *J. Electron. Mater.* **1996**, *25*, 603.

(6) (a) De Melo, O.; Hernandez, L.; Zelaya-Angel, O.; Lozada-Morales, R.; Becerril, M.; Vasco, E. *Appl. Phys. Lett.* **1994**, *65*, 1278. (b) Hernandez, L.; De Melo, O.; Zelaya-Angel, O.; Lozada-Morales, R.; Purón, E. *J. Electrochem. Soc.* **1994**, *141*, 3238. (c) Tornas, S. A.; Vigil, O., Alvarado-Gil, J. J.; Lozada-Morales, R.; Zelaya-Angel, O.; Vargas, H.; Ferreira da Silva, A. *J. Appl. Phys.* **1995**, *78*, 2204. (d) Zelaya-Angel, O.; Hernandez, L.; De Melo, O., Alvarado-Gil, J.; Lozada-Morales, R.; Falcony, C.; Vargas, H.; Ramirez-Bon, R. *Vacuum* **1995**, *46*, 1083. (e) Lozada-Morales, R.; Zelaya-Angel O. *Thin Solid Films* **1996**, *281*, 386.

(7) Bandaranayake, R. J.; Wen, G. W.; Lin, J. Y.; Jiang, H. X.; Sorensen, C. M. *Appl. Phys. Lett.* **1995**, *67*, 831.

(8) Zahn, D. R. T.; Kudlek, G.; Rossow, U.; Hoffmann, A.; Broser, I.; Richter, W. *Adv. Mater. Opt. Electron.* **1994**, *3*, 11.

(9) Yeh, C. Y.; Lu, Z. W.; Froyen, S.; Zunger, A. *Phys. Rev. B: Condens. Matter* **1992**, *46*, 10086.

(10) (a) Kaur, I.; Pandya, D. K.; Chopra, K. L. *J. Electrochem. Soc.* **1980**, *127*, 943. (b) Nakanishi, T.; Ito, K. *Sol. Energy Mater. Sol. Cells* **1994**, *35*, 171.

(11) (a) Froment, M.; Bernard, M. C.; Cortes, R.; Mokili, B.; Lincot, D. *J. Electrochem. Soc.* **1995**, *142*, 2643. (b) Cortes, R.; Froment, M.; Mokili, B.; Lincot, D. *Philos. Mag. Lett.* **1996**, *73*, 209.

(12) (a) Basol, B. M. *Int. J. Sol. Energy* **1992**, *12*, 25. (b) Matsumoto, K.; Takagi, K. *J. Electrochem. Soc.* **1983**, *130*, 423.

(13) (a) Betenekov, N. D.; Medvedev, V. P.; Kitaev, G. A. *Sov. Radiochem.* **1978**, *20*, 369. (b) Nakada, T.; Fukuda, H.; Kunioka, A; Niki, S. *Proceedings of the 13th European Photovoltaic Solar Energy Conference* 1995, 1597. (c) Kylner, A.; Lindgren, J.; Stolt, L. *J. Electrochem. Soc.* **1996**, *143*, 2662.

(14) Khawaja, E.; Tomlin, S. G. *J. Phys. D.: Appl. Phys.* **1975**, *8*, 581.

(15) (a) Özsan, M. E.; Johnson, D. R.; Sadeghi, M.; Sivapathasundaram, D.; Peter, L. M.; Furlong, M. J.; Goodlet, G.; Singleton, A.; Lincot, D.; Mokili, B.; Vedel, J. *Proceedings of the First World Conference Photovoltaic Energy Conversion* **1994**, 327. (b) Özsan, M. E.; Johnson, D. R.; Sadeghi, M.; Sivapathasundaram, D.; Goodlet, G.; Furlong, M. J.; Peter, L. M.; Singleton, A. *J. Mater. Sci.: Mater. Electron.* **1996**, *7*, 119.

(16) (a) De Tacconi, N. R.; Rajeshwar, K. *J. Phys. Chem.* **1993**, *97*, 6504. (b) Leite, R. C. C.; Porto, S. P. S. *Phys. Rev. Lett.* **1966**, *17*, 10. (c) Zahn, D. R. T.; Maierhofer, Ch.; Winter, A.; Reckzugel, M.; Srama, R.; Thomas, A.; Horn, K.; Richter, W. *J. Vac. Sci. Technol. B* **1991**, *9*, 2206.

(17) Blank, H.; Delavignette, P.; Gevers, R., Amelinckx, S. *Phys. Status Solidi A* **1964**, *7*, 747.

(18) Knippenberg, W. F. *Philips Res. Rep.* **1963**, *18*, 161.

(19) Backes, W. H.; Bobbert, P. A.; Van Haeringen, W. *Phys Rev. B: Condens. Matter* **1994**, *49*, 1665.

(20) (a) Engel, G. E.; Needs, R. J. *J. Phys. Rev. B: Condens. Matter* **1990**, *2*, 367. (b) Engel, G. E. *J. Phys. Rev. B: Condens. Matter* **1990**, *2*, 6905. (c) Sebastian, M. T.; Krishna, P. *Philos. Mag. A* **1984**, *49*, 809.

(21) (a) Prasad, S.; Tiwari, B. K.; Srivastava, O. N. *Act. Crystallogr.* **1981**, *A37*, 442. (b) Horodecki, A. J. *Cryst. Res. Technol.* **1987**, *22*, 224.

(22) Bawendi, M. G.; Kortan, A. R.; Steigerwald, M. L.; Brus, L. E. *J. Chem. Phys.* **1989**, *91*, 7282.

(23) Cardona, M.; Weinstein, M.; Wolf, G. A. *Phys. Rev. A: At., Mol., Opt. Phys.* **1965**, *140*, 633.

(24) Kozielski, M. J. *Bull. Acad. Pol. Sci., Ser. Sci. Chim.* **1976**, *24*, 367.

(25) Ernst, P.; Geng, C.; Hahn, G.; Scholz, F.; Schweizer, H.; Phillipp, F.; Mascarenhas, A. *J. Appl. Phys.* **1996**, *79*, 2633.

(26) (a) Froment, M.; Lincot, D. *Electrochim. Acta* **1995**, *10*, 1293. (b) Lincot, D.; Ortega-Borges, R.; Froment, M. *Philos. Mag. B* **1993**, *18*, 185.